PAPER

Check for updates

Helium-induced damage in U$_3$Si$_5$ by first-principles studies†

Yibo Wang,[a] Zhenbo Peng,[b] Nianxiang Qiu,*[a] Heming He,[c] Rongjian Pan, [ID][d] Lu Wu,[d] Qing Huang [ID][a] and Shiyu Du [ID]*[a]

Uranium silicide U$_3$Si$_5$ has been explored as an advanced nuclear fuel component for light water reactor to enhance the accident tolerance. In this paper, in order to understand the fuel performance of U$_3$Si$_5$, the primary point defects, secondary point defects, and the dissolution of He gas were studied by first-principles methods. Compared with U atoms and another type of Si$_2$ atoms, Si$_1$ atoms far from intrinsic Si vacancies are more likely to form point defects, implying that Si vacancies are prone to form separate single vacancies rather than vacancy clusters in the initial stage. From the calculated anti-site defect energies, it can be predicted that non-stoichiometric U-rich phase of U$_3$Si$_5$ are more likely to be formed than Si-rich phase, which are consistent with the chemical analysis of experimentally sintered Si-lean U$_3$Si$_5$ sample. It can be found that a single He atom favors residence in the interstitial site in the U layer directly above/below the intrinsic vacancy. It can also be seen that Vac-U, Vac-Si$_1$, and Vac-Si$_2$ vacancies can energetically accommodate up to 4, 0, and 3 He atoms, respectively. The formation of secondary vacancy defects is strongly dependent on the helium concentration. The current results show that the He-filled vacancy can promote the formation of adjacent secondary vacancy, leading to the formation of gas bubbles. This work may provide theoretical insights into the He irradiation-induced damage in U$_3$Si$_5$ as well as provide valuable clues for improving the design of the UN–U$_3$Si$_5$ composite fuel.

Introduction

After the Fukushima Daiichi accident, the concept of accident tolerant fuels (ATFs) has been proposed in order to provide reliable operational safety.[1] Uranium silicides such as U$_3$Si$_2$ and U$_3$Si$_5$ compounds are being explored as advanced nuclear fuels with higher thermal conductivity and increased fission density, both as stand-alone fuels[2] and as a second phase in composite fuels, compared to the conventional uranium dioxide (UO$_2$) fuel used in the commercial light water reactor (LWR).[3,4] The mechanical, thermo-physical, and thermochemical properties of U–Si compounds such as elastic moduli, heat expansion, heat capacity, thermal conductivity, phase stability, and oxidation reaction are reported experimentally and theoretically.[5–12] Under LWR conditions, point defects, fission products, and the gas species will inevitably continuously change in the fuel

materials, which results in the swelling of the fuel and a reduction in the thermal conductivity and mechanical properties.[6] A number of theoretical studies on the behavior of fission products in U–Si compounds has been reported, including H, H$_2$, Xe, Zr, Sr, Ba, Nd, and Ce.[6–15] Helium, one of the main gases in LWR, has a low diffusion barrier within materials, such as metals and even the MAX phase Ti$_3$AlC$_2$;[16] thus, it tends to aggregate and form bubbles within these materials. However, the He gas behavior in U$_3$Si$_5$, which has one of the very important fuel performance behaviors in U$_3$Si$_5$, are not yet understood.

U$_3$Si$_5$, though having a uranium density (7.5 g U cm^{-3}) lower than both traditional UO$_2$ (9.7 g U cm^{-3}) and U$_3$Si$_2$ (11.3 g U cm^{-3}),[17] and presenting a high melting point (2043 K) compared with those of UO$_2$ (3130 K) and U$_3$Si$_2$ (1983 K),[18] possesses a higher thermal conductivity than UO$_2$ in a broad temperature range from ~573 K to at least 1773 K.[17] In addition, it may have better resistance toward oxidation than U$_3$Si$_2$ by both experimental and theoretical studies.[19,20] Moreover, the UN–U$_3$Si$_5$ composite fuel using U$_3$Si$_5$ as the second phase has received much attention as a potential nuclear fuel material for ATF[4,21] due to its neutronic similarity to UO$_2$ and improved oxidation resistance compared to U$_3$Si$_2$. In our previous theoretical studies,[22] the silicon vacancies of β-USi$_2$ are determined to be more prone to form among the different types of point defects studied and U$_3$Si$_5$ can be treated as a structural derivation of

[a]Engineering Laboratory of Nuclear Energy Materials, Ningbo Institute of Materials Technology and Engineering, Chinese Academy of Sciences, Ningbo, Zhejiang 315201, P. R. China. E-mail: qiunianxiang@nimte.ac.cn; dushiyu@nimte.ac.cn

[b]Institute of Energy Storage & Conversion Technology, Ningbo Polytechnic, China

[c]School of Mechanical and Electrical Engineering, Guangzhou University, Guangzhou 510006, China

[d]The First Sub-Institute, Nuclear Power Institute of China, Chengdu, Sichuan 610005, China

† Electronic supplementary information (ESI) available. See DOI: 10.1039/d1ra04031f

hexagonal β-USi$_2$ with silicon vacancy defects. Furthermore, in contrast to the susceptibility of U$_3$Si$_2$ to ion irradiation-induced amorphization, U$_3$Si$_5$ remains crystalline up to 8 dpa at room temperature and up to ∼50 dpa by 1 MeV Ar^{2+} or 150 keV Kr$^+$ at 623 K,[23] probably due to its more simple and isotropic crystal structure.

In this study, in order to gain a deep insight into the irradiation-induced damage and swelling of the fission gas produced in the fuel, which are valuable for the evaluation of the fuel performance of U$_3$Si$_5$, the behaviors of the fission gas He in U$_3$Si$_5$ are studied by the first-principles method. The primary point defects, secondary vacancies, trapping of He in U$_3$Si$_5$, as well as the volume change associated with He accommodation are discussed. Our results may provide theoretical insights into the solution of He in U$_3$Si$_5$ and provide a valuable clue for improving the design of the UN–U$_3$Si$_5$ composite fuel.

Calculation methods and models

The electronic structure calculations of helium irradiation-induced damage in U$_3$Si$_5$ are performed using projector augmented-wave (PAW) method and Perdew–Burke–Ernzerhof (PBE) functional[24] for exchange-correlation potential implemented in Vienna *Ab initio* Simulation Package (VASP) codes.[25–27] The Hubbard U (PBE + U) method is applied to describe the strong correlation effect of localized uranium 5f orbitals.[28]

U$_3$Si$_5$ has a *P6/mmm* AlB$_2$-type structure, derived from β-USi$_2$ (Fig. 1(a)) by removing one sixth of silicon atoms.[29] Sasa *et al.*[30] suggested that U$_3$Si$_5$ be represented in the form of U$_6$Si$_{10}$ (Fig. 1(b)), as obtained by removing two silicon atoms of the

U$_6$Si$_{12}$ supercell based on β-USi$_2$. Different U values ranging from 0 to 3.5 are tested to obtain a suitable configuration that balances the lattice parameters and stability of U$_3$Si$_5$. The lattice constants of U$_3$Si$_5$ calculations predicted by the PBE + U method agree well with the experiments when $U = 2.5$.[21,31] It is worth noting that the calculated formation energy (−0.462 eV per atom) of U$_3$Si$_5$ also agrees well with the experimental one (−0.45 eV per atom).[20] Moreover, it is experimentally found that U$_3$Si$_5$ is a Curie–Weiss paramagnet above 4.2 K (ref. 32) but becomes non-magnetic below 0.6 K.[33] Also, non-magnetic U$_3$Si$_5$ is theoretically determined to be dynamically stable from the phonon spectrum.[22] Therefore, the non-spin polarized calculation and Hubbard U value of 2.5 are adopted in this study.

Defect configurations are calculated in the $2 \times 2 \times 1$ supercell made up of 64 atoms of U$_6$Si$_{10}$. The plane-wave cutoff energy is set to 500 eV, and $5 \times 5 \times 5$ and $2 \times 2 \times 3$ k-point meshes generated by the Monkhorst–Pack scheme are performed for the U$_6$Si$_{10}$ cell and the U$_{24}$Si$_{40}$ supercell, respectively. The atomic positions, supercell volume, and supercell shape are fully relaxed in all the calculations to obtain the minimum energy structure. The convergence criteria of energy and atomic force are 10^{-6} eV and 0.01 eV Å^{-1}, respectively.

Results and discussion

Point defects and fission products can inevitably be continuously produced in the U$_3$Si$_5$ nuclear fuel under the serving conditions. These defects provide accommodations of fission products and influence the thermo-mechanical properties of the fuel materials. There are two types of Si defects and one type of U defect in U$_3$Si$_5$. The three-point defect types (*i.e.*, Vac-Si$_1$ far from the intrinsic vacancy, Vac-Si$_2$ near intrinsic vacancy, and
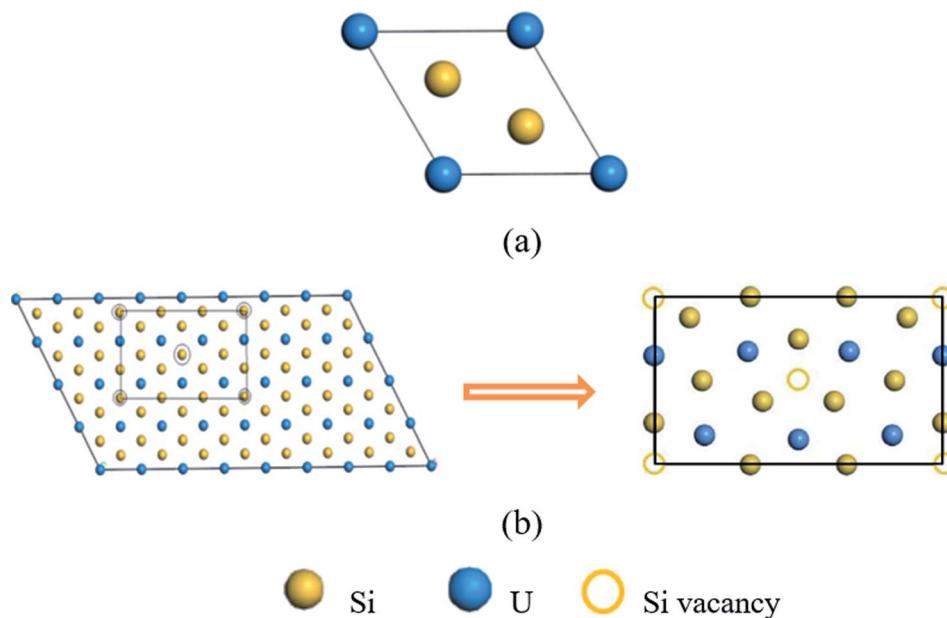

Fig. 1 (a) The crystal structure of hexagonal β-USi$_2$, (b) the crystal structure of orthorhombic U$_6$Si$_{10}$ (marked in the rectangular black line), which is obtained by removing the atoms at the top corners and in the center of the orthorhombic U$_6$Si$_{12}$ crystal, and its corresponding primitive cell is hexagonal U$_3$Si$_5$.

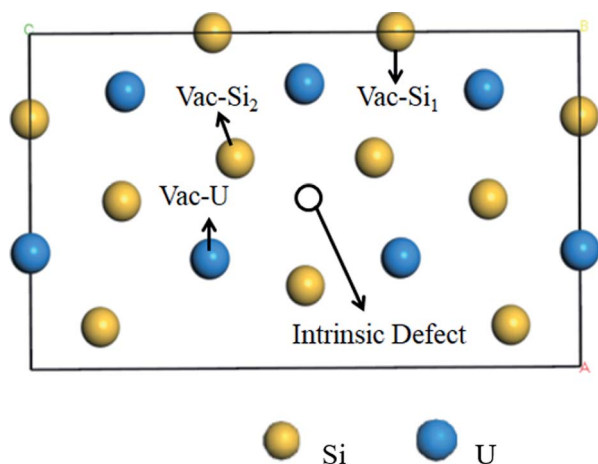**Fig. 2** Schematic diagram of different point defect types in U_3Si_5.

Table 1 Calculated point defect energies and defects formation energies for vacancies and anti-site defects

	Point defect energy	Defect formation energy
Vac-U	8.85	2.10
Vac-Si_1	5.26	0.75
Vac-Si_2	9.86	2.71
Anti-Si_U	2.48	9.68
Anti-U_{Si1}	1.50	−6.08
Anti-U_{Si2}	1.51	−5.91

Vac-U) in Fig. 2 and the three anti-site defect types (Anti-U_{Si1} for substitution of one Si_1 with U, Anti-U_{Si2} for the substitution of one Si_2 with U and Anti-Si_U for the substitution of one U with Si) are investigated in this study. In order to determine the accommodations for gas He, the trapping and secondary defect formation of He into the vacancy defects and/or interstitial defects of U_3Si_5 are also calculated.

In order to assess the stability of vacancies and anti-site defects, the point defect energy E_p^{Vac} and defect formation energy E_f^{Vac} are calculated, respectively, with respect to isolated U or Si atom and silicon in the diamond structure or α-uranium according to ref. 22.

$$E_p^{Vac} = E_{ref}^{Vac} - E_{ref} + E_X \qquad (1)$$

and

$$E_f^{Vac} = E_{ref}^{Vac} - E_{ref} + \mu_X \qquad (2)$$

where E_{ref}/E_{ref}^{Vac} is the total energy of the U_3Si_5 crystal without/with a vacancy, E_X is the energy of an isolated U or Si atom, and μ_X is the elemental chemical potential. For anti-site defects as a common defect type of U–Si compounds, eqn (1) and (2) are modified as follows.

$$E_p^{A_B} = E_{ref}^{A_B} + E_B - E_A - E_{ref} \qquad (3)$$

and

$$E_f^{A_B} = E_{ref}^{A_B} + \mu_B - \mu_A - E_{ref} \qquad (4)$$

here, $E_{ref}^{A_B}$ is the total energy of U_3Si_5 with the substitution of B atom with A atom, E_A and E_B are the respective energies of the isolated A and B atoms, and μ_A and μ_B are the respective elemental chemical potentials of A and B atoms.

The point defect energies and defect formation energies of the vacancies and anti-site defects are summarized in Table 1. Regardless of the defect energies calculated based on the isolated atom as the reference state or the elementary substance as the reference state, Vac-Si_1 is determined to be the lowest and

Vac-Si_2 is the greatest. It can be readily identified that Vac-Si_1 is the most readily produced instead of both Vac-Si_2 and Vac-U adjacent to the intrinsic Si vacancy, which may be an implication of the formation of separated Si vacancies rather than the vacancy clusters. It can be also seen that Vac-U is slightly more likely to be produced than Vac-Si_2, even though the U atomic radius is larger than that of Si. This current result is consistent with the finding of the U_3Si_2 system.[13,34] This observation can be understood in that the intrinsic defect of U_3Si_5 slightly elongates the Si–Si bond length and weakens the bond strength so that Vac-Si_1 is more likely to be formed than Vac-U. However, the removal of the Si_2 atom to form the bivacancy defect could locally disturb the U_3Si_5 structure and increase the energy of the system. As for the anti-site defects, it can be noted that Anti-U_{Si1}/Anti-U_{Si2} have lower defect energies than Anti-Si_U, which indicates that the non-stoichiometric U-rich phase of U_3Si_5 is more likely to be sintered than the Si-rich phase, which is consistent with the chemical analysis of the experimentally sintered Si-lean U_3Si_5 sample.[17] In addition, the defect formation energies of Anti-U_{Si1} and Anti-U_{Si2} are similar and both are negative, which may also be a sign of the U-rich phase present in the U_3Si_5 sample.

To identify the preferential site for a single He atom residing in perfect or defect U_3Si_5, the solution energy of He trapped in U_3Si_5 without and with point defects is calculated by ref. 35 and 36.

$$E^s(He) = E_{ref}^{He} - E_{ref} - E(He) \qquad (5)$$

where E_{ref}^{He} (E_{ref}) is the energy of perfect or defect U_3Si_5 with (without) an He atom, and $E(He)$ is the energy of an isolated He atom. The trap sites of He occupying U_3Si_5 with the anti-site defect are not included because the swelling of non-stoichiometric U_3Si_5 is beyond the content of the present study. Helium accommodation into the interstitial sites of U_3Si_5 with the space group of $P\bar{6}2m$ is investigated to determine the preferential interstitial site. There are six types of interstitial sites considered in Fig. 3, *i.e.*, the intrinsic vacancy as an interstitial site 1b (0.0, 0.0, 0.5) in the Si layer, 1a (0.0, 0.0, 0.0) site in the U layer directly below or above the intrinsic vacancy, pentagonal bipyramidal 3g (0.3635, 0.3635, 0.50) site in the Si layer between two U atoms, 3f (0.2486, 0.0, 0.0) site in the U layer between two Si_2 atoms, trigonal bipyramidal 2c (2/3, 1/3, 0.0) site in the U layer between two Si_1 atoms, and 6i (0.5575, 0.5575,
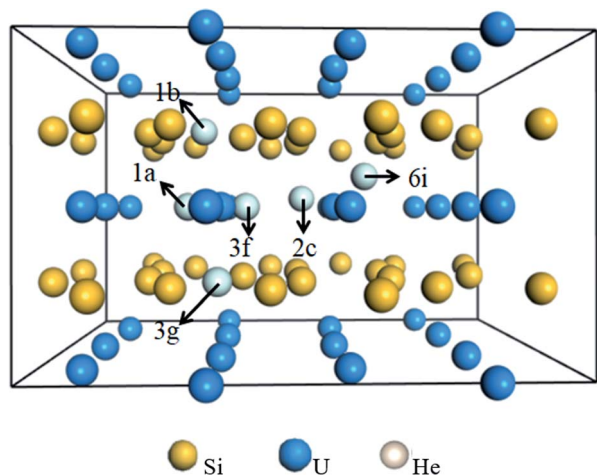
Fig. 3 The initial structure with a single He atom accommodated in one of the six types of interstitial sites, *i.e.*, intrinsic vacancy as an interstitial site 1b in the Si layer, 1a site in the U layer directly above/below the intrinsic vacancy, 3g site in the Si layer between two U atoms, 3f site in the U layer between two Si$_2$ atoms, 2c site in the U layer between two Si$_1$ atoms, and 6i site between adjacent U and Si layers.

0.25) site between adjacent U and Si layers. The solution energies of single He incorporation into the interstitial sites are summarized in Table 2. It can be readily identified that the lowest solution energy interstitial site for a single He is to be located in 1a instead of the intrinsic vacancy 1b. It could be interesting to point out that the 1a site in the U layer has a larger free volume for He accommodation as compared to the 1b site due to the longer U–U bond. Moreover, the introduction of the intrinsic Si vacancy eliminates the repulsion of helium atoms residing in the U atomic layer from the nearest Si atoms. By comparing the calculated interstitial site solution energy, it can be concluded that the interstitial site 1a below or above the intrinsic vacancy provides a good sink for He accommodation.

It is well known that the lattice constants and volume will change when a fission gas is accommodated. The changes in the lattice constants and volume for He accommodated in the interstitial sites are listed in Table A1.† Compared to the perfect U$_3$Si$_5$, the volume associated with He residing in the interstitial

Table 2 The solution energies of He incorporation into various interstitial sites investigated

Wyckoff position	Solution energy (eV)	Comment
1b	2.081	Relaxed to 1a
1a	2.074	
3g	5.085	A neighboring U atom is relaxed to the adjacent Si atomic layer
3f	2.086	Relaxed to 1a
2c	2.856	
6i	2.762	A neighboring Si$_2$ atom is relaxed to an intrinsic vacancy

site anisotropically expands from 0.43% for the 1a site to 1.99% for the 3g site. It can also be seen that the order of volume change is consistent with that of single He interstitial solution energy and the volume expansion associated with He trapped in the 1a site is estimated to be the lowest among the interstitials investigated. This means that the He gas incorporated into the 1a site in the U layer above/below the adjacent intrinsic vacancy causes the lowest strain on the U$_3$Si$_5$ structure, resulting in the smallest solution energy.

The solution energies of a single He incorporated into the three types of vacancies in U$_3$Si$_5$ are also predicted to assess their ability of He accommodation. The calculated helium vacancy solution energies at Vac-Si$_1$, Vac-U, and Vac-Si$_2$ are 2.59, 1.96, and 0.47 eV, respectively, which are in contrast with the defect formation energies of the corresponding vacancies but appear to be inversely proportional to the vacancy volume because Vac-Si$_2$ coupled with the intrinsic vacancy has the largest free volume among the vacancies studied, then Vac-U with a U vacancy, and finally Vac-Si$_1$ with a Si$_1$ vacancy. It is also interesting to point out that the introduction of vacancy reduces the solution energy of He in the adjacent interstitial site closest to the vacancy by increasing the residence volume. For example, the respective solution energies of He residing in the Vac-U and Vac-Si$_1$ are smaller than that of the interstitial sites 1a and 2c, respectively. Therefore, it can be reasonably inferred that the trapping of helium into the vacancy is dominated by entropy. In addition, the filling of the interstitial site 1a directly above the intrinsic vacancy or Vac-Si$_2$ coupled with the intrinsic vacancy with an He atom is found to be the most favorable. This is an indication that the intrinsic vacancies of the U$_3$Si$_5$ structure helps to provide a good sink or become a part of a good sink for the fission gas, which provides an explanation of the exceptional stability of U$_3$Si$_5$ against ion radiation damage made from the experimental work by Y. Sasa *et al.*[30]

In order to obtain the number of He atoms accommodated in the three types of vacancies investigated, we calculated the trapping energy of an additional He atom residing in the vacancy using eqn (6).[35,36]

$$E_{\text{trap}} = E_{\text{U}_3\text{Si}_5}(n\text{He, V}) - E_{\text{U}_3\text{Si}_5}((n-1)\text{He, V}) - E_{\text{U}_3\text{Si}_5}(\text{He, 1a}) + E_{\text{U}_3\text{Si}_5} \quad (6)$$

where $E_{\text{U3Si5}}n$He, V is the energy of the U$_3$Si$_5$ system with a single vacancy and nHe atoms and E_{U3Si5}He, 1a is the energy of U$_3$Si$_5$ with a single He atom residing in the interstitial site 1a in the U layer, which is determined to be the most favorable trap site in the perfect U$_3$Si$_5$ structure. A negative E_{trap} value means that it is energetically more favorable to fill an additional He atom into the vacancy discussed than the interstitial site 1a of the perfect U$_3$Si$_5$. The dependence of the trapping energy on the number of He atoms in Vac-U, Vac-Si$_1$, and Vac-Si$_2$ vacancies is depicted in Fig. 4. The trapping energy of an He atom in Vac-Si$_1$ is positive, showing that the He atom prefers to stay in the interstitial site 1a of the perfect U$_3$Si$_5$ rather than Vac-Si$_1$, and, in other words, it is difficult for He atoms to aggregate in Vac-Si$_1$. It is energetically favorable for Vac-U to accommodate four He atoms. It can be seen from the insets of Fig. 4 that the four
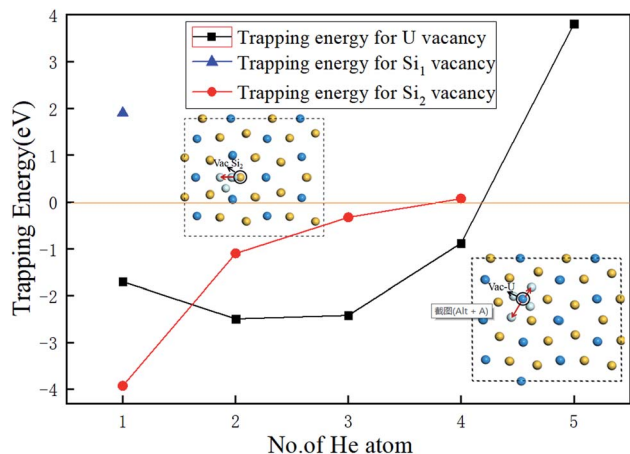
Fig. 4 The dependence of the trapping energy on the number of He atoms trapped in Vac-U, Vac-Si$_1$, and Vac-Si$_2$ vacancies of U$_3$Si$_5$.

He atoms tend to reside in the U layer near the Vac-U vacancy. But when the fifth He atom is implanted, the trapping becomes unfavorable because the corresponding trapping energy becomes positive. Also, for Vac-Si$_2$, the preferential trapping is for the first three He atoms to reside in the interstitial site 1a and between the U and Si layers near the Vac-Si$_2$ of U$_3$Si$_5$. Therefore, Vac-U, Vac-Si$_1$, and Vac-Si$_2$ vacancies can energetically accommodate up to 4, 0, and 3 He atoms relative to the interstitial site 1a of U$_3$Si$_5$, respectively. It can be seen from Fig. A3† that chain-like bubbles are formed when three He gas are implanted into the primary Si$_2$ vacancy. Also, in Fig. A4,† the 4He atoms implanted are distributed in the plane of the U atomic layer. It can also be concluded that helium atoms reside as an individual atom in Vac-Si$_1$ and interstitial sites or combine with the Vac-U and Vac-Si$_2$ vacancies to form the gas bubbles, in accordance with the experimental observations.[30]

In order to more deeply understand the influence of the crystal structure of U$_3$Si$_5$ on the number of implanted He atoms, the lattice constants and volume as increasing number of He atoms are summarized in Table 3. When a U or Si vacancy is introduced, the volume and lattice parameters a and c exhibit a weak contraction while the lattice parameter b expands. This can be explained by the fact that when a U or Si atom is removed, the adjacent U or Si atoms in the U or Si layer on the $a/$

c plane move closer to the vacancy, causing the lattice constants a and c to shrink, while the loss of U–Si bonds along the b-axis makes the structure expand along the b-axis direction. It is interesting to point out that when one He atom is implanted into a U vacancy, the volume continues to shrink anisotropically by −2.37%, which may cause the compression of the structure, resulting in a small trapping energy in Fig. 4, and the change of the b value increases from 1.69% to 3.14%. However, when there are more than one He atoms implanted, although the parameters a and c still shorten relative to U$_3$Si$_5$, the volume expands instead from 0.063% for two He atoms to 2.58% for 4He atoms. This means that the tensile strength of U$_3$Si$_5$ along the b-axis becomes the dominant factor as the implanted He atoms increase, thereby increasing the system energy and reducing the trapping energy, as depicted in Fig. 4. From Table 3, the structural variant of U$_3$Si$_5$ with Vac-Si$_2$ and implanted He atoms is slightly different from that of Vac-U. It can be clearly seen that when He atoms are trapped in Vac-Si$_2$, the lattice constants all show an expansion except for the lattice constant b associated with two implanted He atoms. Thus, the corresponding crystal volume enlarges by 0.45%, associated with one trapped He to 1.21% associated with three trapped He. It can be found carefully that as the implanted He increases, the rapid expansion along the c-axis may destroy the strong silicon–silicon covalent bonds and uranium–uranium metallic bonds, thereby increasing the instability of the system, resulting in the He trapping ability of the Vac-Si$_2$ vacancy being weaker than that of the Vac-U vacancy. Therefore, it provides a structural understanding of the evolution of the He trapping ability in different types of vacancies by varying the number of He atoms implanted.

To further study the evolution of helium bubble-induced defect structure of U$_3$Si$_5$, the secondary point defects (nearest U, nearest Si$_1$, and nearest Si$_2$) nearest to the primary vacancies with the trapped He atoms discussed above are investigated and the corresponding secondary defect formation energies are provided in Fig. 5 according to ref. 35 and 36.

$$E_f^2(V_A) = E(V_{A+B}) - E(V_B) + \mu_A \tag{7}$$

Here, $E(V_{A+B})$ is the total energy of the system with one primary vacancy B and one secondary vacancy A, $E(V_B)$ is the

Table 3 Lattice constants and volume associated with different number of He atoms trapped in Vac-U and Vac-Si$_2$

| Structures	a (Å)	b (Å)	c (Å)	V (Å^3)	$\Delta a/a$ (%)	$\Delta b/b$ (%)	$\Delta c/c$ (%)	$\Delta V/V$ (%)
U$_3$Si$_5$	13.231	8.048	11.397	1213.64	0	0	0	0
Vac-U	13.032	8.184	11.265	1201.54	−1.505	1.690	−1.161	−0.997
Vac-U + 1He	12.810	8.301	11.142	1184.90	−3.181	3.144	−2.237	−2.368
Vac-U + 2He	13.025	8.293	11.243	1214.41	−1.557	3.040	−1.351	0.063
Vac-U + 3He	13.122	8.309	11.326	1234.92	−0.824	3.243	−0.824	1.753
Vac-U + 4He	13.055	8.439	11.299	1244.97	−1.330	4.858	−1.330	2.581
Vac-Si$_2$	12.869	8.288	11.144	1188.57	−2.736	2.982	−2.220	−0.207
Vac-Si$_2$ + 1He	13.255	8.086	11.399	1219.06	0.181	0.472	0.0175	0.447
Vac-Si$_2$ + 2He	13.201	8.071	11.447	1219.66	−0.227	0.286	0.439	0.496
Vac-Si$_2$ + 3He	13.270	8.050	11.498	1228.27	0.295	0.025	0.886	1.205
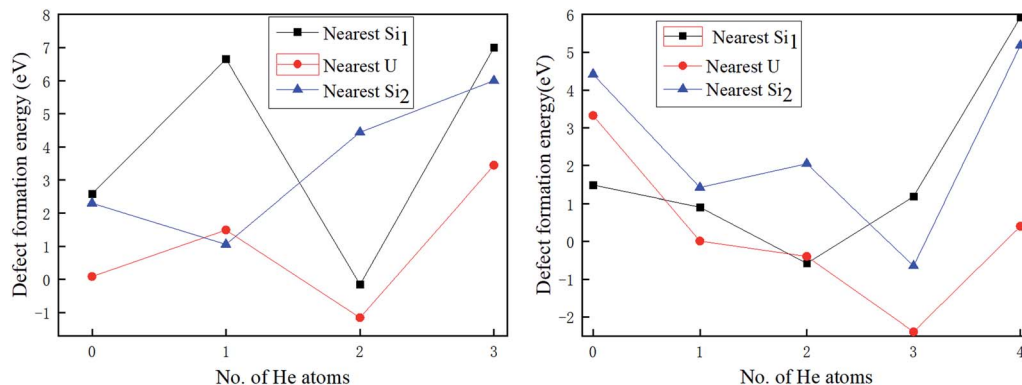
Fig. 5 The secondary defect formation energies for nearest Si_1, nearest U, and nearest Si_2 adjacent to a primary Si_2 vacancy (a) and a primary U vacancy (b) as a function of the number of implanted He atoms.

energy of the system that contains one vacancy of type B, and μ_A is the elemental chemical potential of species A.

One can see from Fig. 5 that the formation of secondary defects is strongly dependent on the helium concentration. When there is no He atom residing in the primary Vac-Si_2, the respective secondary defect formation energies of the nearest U, nearest Si_1, and nearest Si_2 are 0.087, 2.57, and 2.30 eV, respectively, which is an implication that the nearest U vacancy induced by primary Vac-Si_2 is much more likely to be produced than nearest Si_1 and nearest Si_2. With the increase in the He atoms trapped, the secondary defect formation energy of the nearest Si_2 almost continues to increase to 6.00 eV with three He atoms, which is the maximum number of He atoms residing in Vac-Si_2 because the He atoms implanted near Vac-Si_2 have a strong interaction with the nearest Si_2 so that the removal of the nearest Si_2 is prevented in Fig. A1b.† However, there is an obvious exception for nearest U and nearest Si_1, where the respective defect formation energy drops dramatically to −1.16 and −0.16 eV when the two He atoms are accommodated. This means that 2He-filled Vac-Si_2 can promote the spontaneous formation of nearest U and nearest Si_1. By contrast, it would be interesting to note that the fully filled Vac-Si_2 can significantly raise the secondary defect formation energy to at least 3.44 eV (for nearest U). From the above analysis, once the Vac-Si_2 vacancy of U_3Si_5 is formed under the serving conditions; the U vacancy nearest to the Vac-Si_2 is prone to be produced in terms of the secondary defect formation energy. When the He-filled Vac-Si_2 has secondary defects, the chain-like bubbles containing volume of interstitial site 1a and Vac-Si_2 are formed, while the secondary U of the adjacent U layer and Si_1 of the same Si layer nearest to the 2He-filled Vac-Si_2 could be formed spontaneously, resulting in a three-dimensional (spherical) defect structure, which will also lead to the formation of spherical bubbles.

As shown in Fig. 5(b), when no He atom enters the primary Vac-U vacancy, the secondary defect formation energy of the nearest Si_1 is positive and the smallest among the secondary vacancies is studied, indicating that it prefers to form U–Si_1 bivacancy. With the increase in the helium atoms implanted, all the secondary defect formation energies of the nearest Si_1,

nearest U, and nearest Si_2 roughly decrease first and then increase. As in the case of Vac-Si_2, fully 4He-filled Vac-U shown in Fig. A2† will significantly enhance the stability of the structure and prevent the generation of nearby defects. However, the secondary defect formation energy of the nearest Si_1 becomes negative and reaches a minimum of −0.58 eV when two He atoms exist, while those of the nearest U and Si_2 reach the minimum values (−2.39 eV for nearest U and −0.65 eV for nearest Si_2) when the third He atom is placed at these vacancies, which can be explained by the fact that the Vac-U and Vac-Si_2 vacancies have much smaller He solution energies than Vac-Si_1 and thus provide a better sink for the third He atom. In other words, the partially filled Vac-U can also promote the spontaneous formation of the secondary defects Si_1 and Si_2 of the adjacent Si layer as well as U of the same U layer, and thus generate both three- and two-dimensional vacancy structures, i.e., plate-like and spherical bubbles. For the fully He-filled Vac-U, the development of the secondary defects is prevented and the plate-like bubbles will be formed with high probability, which is similar to the gas bubble structure of an irradiated U_3Si_2 dispersion fuel made from the experimental work.[10]

Conclusions

In this paper, the behaviors of the fission gas He in U_3Si_5 are studied by the first-principles method. The primary point defects, secondary point defects, and the dissolution of fission gas He are studied. The results show that the defect formation energies of the point defects investigated follow the order Si_2 > U > Si_1, indicating that Vac-Si_1 is more likely to form, and Si vacancies are prone to form separate single vacancies rather than vacancy clusters. It can be found that the non-stoichiometric U-rich phase of U_3Si_5 is more likely to be formed than the Si-rich phase, which is consistent with the chemical analysis of the experimentally sintered Si-lean U_3Si_5 sample. By comparing the calculated interstitial site solution energy, it can be concluded that the interstitial site 1a below or above the intrinsic vacancy provides a good sink for He accommodation. It can be also seen that Vac-U, Vac-Si_1, and Vac-Si_2 vacancies can energetically accommodate up to 4, 0, and

3 He atoms relative to the interstitial site 1a, respectively. In addition, although the fully He-filled primary vacancy can prevent the growth of the secondary defects, partially He-filled vacancy can promote the formation of an adjacent secondary vacancy, leading to the formation of three-dimensional spherical gas bubbles. This work may provide a theoretical insight into the He irradiation-induced damage in U_3Si_5 as well as provide valuable clues for improving the design of the $UN–U_3Si_5$ composite fuel.

Conflicts of interest

The authors declare no competing financial interest.

Acknowledgements

References

1 S. J. Zinkle and G. S. Was, Materials challenges in nuclear energy, *Acta Mater.*, 2013, **61**(3), 735–758, DOI: 10.1016/j.actamat.2012.11.004.

2 S. J. Zinkle, K. A. Terrani, J. C. Gehin, L. J. Ott and L. L. Snead, Accident tolerant fuels for LWRs: A perspective, *J. Nucl. Mater.*, 2014, **448**(1–3), 374–379, DOI: 10.1016/j.jnucmat.2013.12.005.

3 K. D. Johnson, A. M. Raftery, D. A. Lopes and J. Wallenius, Fabrication and microstructural analysis of $UN-U_3Si_2$ composites for accident tolerant fuel applications, *J. Nucl. Mater.*, 2016, **477**, 18–23, DOI: 10.1016/j.jnucmat.2016.05.004.

4 N. R. Brown, M. Todosow and A. Cuadra, Screening of advanced cladding materials and $UN–U_3Si_5$ fuel, *J. Nucl. Mater.*, 2015, **462**, 26–42, DOI: 10.1016/j.jnucmat.2015.03.016.

5 Y. Zhang and A. D. R. Andersson, *A Thermal Conductivity Model for U-Si Compounds*, LA-UR-16-27736, 2017, vol. 02, pp. 1–9, DOI: 10.2172/1342838.

6 Y. Miao, *et al.*, "Gaseous swelling of U_3Si_2 during steady-state LWR operation: A rate theory investigation", *Nucl. Eng. Des.*, 2017, **322**, 336–344, DOI: 10.1016/j.nucengdes.2017.07.008.

7 Y. Miao, K. A. Gamble, D. Andersson, Z. G. Mei and A. M. Yacout, Rate theory scenarios study on fission gas behavior of U_3Si_2 under LOCA conditions in LWRs, *Nucl. Eng. Des.*, 2018, **326**, 371–382, DOI: 10.1016/j.nucengdes.2017.11.034.

8 S. C. Middleburgh, P. A. Burr, D. J. M. King, L. Edwards, G. R. Lumpkin and R. W. Grimes, Structural stability and fission product behaviour in U_3Si, *J. Nucl. Mater.*, 2015, **466**, 739–744, DOI: 10.1016/j.jnucmat.2015.04.052.

9 Y. Miao, *et al.*, "Bubble morphology in U_3Si_2 implanted by high-energy Xe ions at 300 °C", *J. Nucl. Mater.*, 2017, **495**, 146–153, DOI: 10.1016/j.jnucmat.2017.07.066.

10 Y. S. Kim, G. L. Hofman, J. Rest and A. B. Robinson, Temperature and dose dependence of fission-gas-bubble swelling in U_3Si_2, *J. Nucl. Mater.*, 2009, **389**(3), 443–449, DOI: 10.1016/j.jnucmat.2009.02.037.

11 T. Barani, *et al.*, "Multiscale modeling of fission gas behavior in U_3Si_2 under LWR conditions", *J. Nucl. Mater.*, 2019, **522**, 97–110, DOI: 10.1016/j.jnucmat.2019.04.037.

12 T. Winter and C. Deo, Comparison of fission gas swelling models for amorphous U_3Si_2 and crystalline UO_2, *Ann. Nucl. Energy*, 2017, **100**, 31–41, DOI: 10.1016/j.anucene.2016.08.008.

13 A. D. Andersson, *"Density Functional Theory Calculations of Defect and Fission Gas Properties in U–Si Fuels"*, 2016, vol. 03, doi: DOI: 10.2172/1237246.

14 T. Yao, B. Gong, L. He, J. Harp, M. Tonks and J. Lian, Radiation-induced grain subdivision and bubble formation in U_3Si_2 at LWR temperature, *J. Nucl. Mater.*, 2018, **498**, 169–175, DOI: 10.1016/j.jnucmat.2017.10.027.

15 D. A. Andersson, X. Y. Liu, B. Beeler, S. C. Middleburgh, A. Claisse and C. R. Stanek, Density functional theory calculations of self- and Xe diffusion in U_3Si_2, *J. Nucl. Mater.*, 2019, **515**, 312–325, DOI: 10.1016/j.jnucmat.2018.12.021.

16 Y. Xu, *et al.*, "New insight into the helium-induced damage in MAX phase Ti_3AlC_2 by first-principles studies", *J. Chem. Phys.*, 2015, **143**(11), DOI: 10.1063/1.4931398.

17 J. T. White, A. T. Nelson, D. D. Byler, D. J. Safarik, J. T. Dunwoody and K. J. McClellan, Thermophysical properties of U_3Si_5 to 1773 K, *J. Nucl. Mater.*, 2015, **456**, 442–448, DOI: 10.1016/j.jnucmat.2014.10.021.

18 V. S. Yemel'Yanov and A. L. Yevstyukhin, *Metall. Nucl. Fuel.*, 1969.

19 A. T. Nelson, J. T. White, D. D. Byler, J. T. Dunwoody, J. A. Valdez and K. J. McClellan, Overview of properties and performance of uranium-silicide compounds for light water reactor applications, *Trans. Am. Nucl. Soc.*, 2014, **110**, 987–989.

20 C. K. Chung, *et al.*, "Enthalpies of formation and phase stability relations of USi, U_3Si_5 and U_3Si_2", *J. Nucl. Mater.*, 2019, **523**, 101–110, DOI: 10.1016/j.jnucmat.2019.05.052.

21 K. James, *FY2016 Ceramic Fuels Development Annual Highlights*, 2016, vol. 05.

22 X. Zhang, *et al.*, "Electronic structures, mechanical properties and defect formation energies of U_3Si_5 from density functional theory calculations", *Prog. Nucl. Energy*, 2019, **116**, 87–94, DOI: 10.1016/j.pnucene.2019.03.045.

23 T. Yao, *et al.*, "*In situ* TEM study of the ion irradiation behavior of U_3Si_2 and U_3Si_5", *J. Nucl. Mater.*, 2018, **511**, 56–63, DOI: 10.1016/j.jnucmat.2018.08.058.

24 J. P. Perdew, K. Burke and M. Ernzerhof, Generalized gradient approximation made simple, *Phys. Rev. Lett.*, 1996, **77**(18), 3865–3868, DOI: 10.1103/PhysRevLett.77.3865.

25 G. Kresse and J. Hafner, *Ab initio* molecular dynamics for liquid metals, *Phys. Rev. B: Condens. Matter Mater. Phys.*, 1993, **47**(1), 558–561, DOI: 10.1103/PhysRevB.47.558.

26 G. Kresse and J. Furthmüller, Efficiency of *ab initio* total energy calculations for metals and semiconductors using a plane-wave basis set, *Comput. Mater. Sci.*, 1996, **6**(1), 15–50, DOI: 10.1016/0927-0256(96)00008-0.

27 G. Kresse and J. Furthmüller, Efficient iterative schemes for *ab initio* total-energy calculations using a plane-wave basis set, *Phys. Rev. B: Condens. Matter Mater. Phys.*, 1996, **54**(16), 11169–11186, DOI: 10.1103/PhysRevB.54.11169.

28 S. Dudarev and G. Botton, Electron-energy-loss spectra and the structural stability of nickel oxide: An LSDA+U study, *Phys. Rev. B: Condens. Matter Mater. Phys.*, 1998, **57**(3), 1505–1509, DOI: 10.1103/PhysRevB.57.1505.

29 A. Brown and J. J. Norreys, "Uranium Disilicide", *Nature*, 1961, **191**, 61–62, DOI: 10.1038/191061a0.

30 Y. Sasa and M. Uda, Structure of stoichiometric USi_2, *J. Solid State Chem.*, 1976, **18**(1), 63–68, DOI: 10.1016/0022-4596(76)90079-7.

31 S. Auffret, J. Pierre, B. Lambert, J. L. Soubeyroux and J. A. Chroboczek, Crystallographic and magnetic structures of Er_3Si_5, *Phys. B*, 1990, **162**(3), 271–280, DOI: 10.1016/0921-4526(90)90022-m.

32 T. Miyadai, *et al.*, "Magnetic and electrical properties of the U-Si system (part II)", *J. Magn. Magn. Mater.*, 1992, **104–107**(1), 47–48, DOI: 10.1016/0304-8853(92)90697-M.

33 N. Sato, M. Kagawa, K. Tanaka, N. Takeda, T. Satoh and T. Komatsubara, Magnetic properties of a mass-enhanced ferromagnet U_2PtSi_3, *J. Magn. Magn. Mater.*, 1992, **108**, 115–116, DOI: 10.1016/0304-8853(92)91373-2.

34 T. Wang, *et al.*, "First-principles investigations on the electronic structures of U_3Si_2", *J. Nucl. Mater.*, 2016, **469**, 194–199, DOI: 10.1016/j.jnucmat.2015.11.060.

35 C. Duan, *et al.*, "First-principles study on dissolution and diffusion properties of hydrogen in molybdenum", *J. Nucl. Mater.*, 2010, **404**(2), 109–115, DOI: 10.1016/j.jnucmat.2010.06.029.

36 Y. L. Liu, Y. Zhang, H. B. Zhou, G. H. Lu, F. Liu and G. N. Luo, Vacancy trapping mechanism for hydrogen bubble formation in metal, *Phys. Rev. B: Condens. Matter Mater. Phys.*, 2009, **79**(17), 1–4, DOI: 10.1103/PhysRevB.79.172103.